Biological Trace Element Research (2022) 200:931–942
https://doi.org/10.1007/s12011-021-02697-z

Synthesis of Silver- and Strontium-Substituted Hydroxyapatite with Combined Osteogenic and Antibacterial Activities

Yunfei Li[1] · Wenying Wang[1] · Jing Han[1] · Zirui Li[1] · Qiuxiang Wang[1] · Xue Lin[1] · Kun Ge[1] · Guoqiang Zhou[1,2]

Received: 19 February 2021 / Accepted: 28 March 2021 / Published online: 2 April 2021

Abstract

Infection in bone transplantation process is attracting considerable attention. The current study synthesizes silver/strontium co-substituted hydroxyapatite (Ag/Sr-HA) nanoparticles with combined osteogenic and antibacterial activities. Different concentrations of silver-substituted hydroxyapatite (Ag-HA) nanoparticles were synthesized by hydrothermal method, and then their physicochemical properties were characterized by X-ray powder diffraction (XRD), Fourier transform infrared spectroscopy (FTIR), transmission electron microscope (TEM), and energy-dispersive X-ray spectroscopy (EDS). Then, Sr was added as secondary element into Ag-HA to improve the biocompatibility of substrate. The antibacterial experiments indicated that Ag-HA had excellent antibacterial activity against Escherichia coli (E. coli) and Staphylococcus aureus (S. aureus). The effects of prepared samples on cell proliferation and differentiation were evaluated using MC3T3-E1 cells in vitro. The results showed that Sr substitution enhanced cell proliferation and differentiation, upregulated expression of osteogenic genes, and induced mineralization of cells. The substitution of Sr in Ag/Sr-HA nanoparticles can effectively alleviate the negative effects of Ag and enhance the biological activity of HA. Thus, the synthesized Ag/Sr-HA nanoparticles will serve as a potential candidate for application of biomedical implants with excellent osteogenic and antibacterial ability.

Keywords Hydroxyapatite · Strontium · Silver · Osteogenic ability · Antibacterial activity

Introduction

Hydroxyapatite (HA) has been widely used in orthopedics and dentistry to enhance bone regeneration due to its excellent bioactivity, biocompatibility, and osteoinductivity [1, 2]. It has been also applied as a cladding material of metal implants for its ability to promote cellular functions and osteoinductivity [3, 4]. The major risk factor during implanting process is postoperative infection, which usually leads to severe pain and implant failure [5]. The local implants have no lasting antimicrobial effects during bone regeneration [6]. Microbial infections should be managed in first during transplantation. So lack of antibacterial activity is a limitation of HA used in tissue engineering. The antibacterial property should be introduced into HA for more successful implants. Various types of antibacterial materials included silver (Ag), zinc oxide (ZnO), and copper (Cu) have been reported to be useful with their antibacterial activity [7, 8]. The incorporation of inorganic antimicrobials such as Ag, ZnO, and Cu in biological grafting materials is a strategy to prevent microbial infection [9–11]. Among these antibacterial materials, Ag has excellent antibacterial activity against several kinds of bacteria and also nontoxic to mammalian and prokaryotic cells at low concentration [12, 13]. Ag has been incorporated into some compounds to enhance the antimicrobial activity. Previous studies have shown that the higher proportion of Ag in these substrates gives better antibacterial effects but with increasing cytotoxicity [14]. Therefore, a secondary chemical element needs to be introduced to mitigate negative effects and retain antibacterial activities of the substrate materials.

Some trace metal elements included magnesium (Mg), zinc (Zn), and Cu can promote bone formation. As an important trace element in bone, Mg plays a special role in bone restoration process. It has been demonstrated that Ag/Mg-HA had better antibacterial activity and osteoinductive ability [15]. The incorporation of Mg effectively lessened the negative

✉ Guoqiang Zhou
zhougq@hbu.edu.cn

[1] Key Laboratory of Medicinal Chemistry and Molecular Diagnosis of Ministry of Education, Key Laboratory of Chemical Biology of Hebei Province, College of Chemistry and Environmental Science, Hebei University, Baoding 071002, China

[2] Key Laboratory of Pathogenesis Mechanism and Control of Inflammatory-autoimmune Diseases of Hebei Province, College of Basic Medical Sciences, Hebei University, Baoding 071000, China

effects and improved the biocompatibility of Ag-HA. Similarly, the Zn/Ag co-implanted titanium not only promoted the adhesion, spreading, proliferation, and osteogenic differentiation of rBMSCs, but also exhibited excellent antibacterial ability [16]. With excellent bioactivity and antimicrobial ability, Cu-doped bioactive glass nanoparticles provided potential applications in the prevention of infectious diseases and treatment of bone defects [17]. Strontium (Sr) is a natural element in human body with bone targeting property and has attracted an extensive interest in the bone injuries management due to its effective antiosteoporosis activity [18]. Sr plays an important role in the early stages of osteogenesis, which inhibits bone resorption, increases bone formation, promotes osteoblastic differentiation, stimulates the expression of type I collagen protein and dental matrix protein I while increasing the secretion of osteoprotegerin [19–22]. Hence, Sr is an encouraging auxiliary chemical for mitigating the potential adverse impact of Ag-HA. The new compound may exhibit excellent antibacterial activity and acceptable biocompatibility in bone tissues after incorporation of Sr and Ag into HA.

In this study, a series of Ag and Sr co-substituted HA nanoparticles were synthesized by a hydrothermal method. The antibacterial activity and cell viability of HA doped with different concentrations of Ag were studied. Then, Ag/Sr-HA co-substituted with fixed concentration (5.0 wt.%) of Ag and four different concentrations (1.0, 2.5, 5.0, and 10.0 wt.%) of Sr was synthesized to improve the antibacterial and osteogenic activity of HA. The antimicrobial properties of HA, Ag-HA, and Ag/Sr-HA were performed in interaction with microbial cultures of E. coli and S. aureus in vitro. Then the effects of prepared samples on cell proliferation and differentiation were analyzed using MC3T3-E1 cells in vitro. The results showed that Ag incorporation improved antibacterial activity of HA significantly. The incorporation of Sr enhanced cell proliferation and differentiation, upregulated expression of osteogenic genes, and induced mineralization of cells. The substitution of Sr in Ag/Sr-HA nanoparticles can effectively alleviate negative effects of Ag and enhance osteogenic activity of HA. The Ag/Sr-HA is a potential candidate for many biomedical applications in implants due to its improved osteogenic and antibacterial properties.

Materials and Methods

Materials and Reagents

Calcium nitrate tetrahydrate ($Ca(NO_3)_2$•$4H_2O$), silver nitrate ($AgNO_3$), strontium nitrate tetrahydrate ($Sr(NO_3)_2$•$4H_2O$), ethylenediamine tetraacetic acid disodium (EDTA disodium), ammonia solution (NH_3•H_2O), and diammonium hydrogen phosphate ($(NH_4)_2HPO_4$), were purchased from Kemiou Chemical Reagent Co. Ltd. (Tianjin, China). The osteoblast precursor MC3T3-E1 cell line was purchased from the Institute of Cell Research of Chinese Academy of Sciences (Shanghai, China). 3-(4,5-Dimethylthiazol-2-yl)-2,5-diphenyl tetrazolium bromide (MTT), β-glycerophosphate, penicillin, streptomycin, dexamethasone, collagen II, ascorbic acid, insulin, alizarin red-S (ARS), cetylpyridium chloride, and dimethylsulfoxide (DMSO) were obtained from Sigma-Aldrich (St. Louis, USA). Alpha-modified Eagle's medium (α-MEM), fetal Bovine Serum (FBS), and trypsin were purchased from Gibco (Grand Island, NY, USA). All the other chemical reagents were analytical grade and used without further purification.

Synthesis of Nanoparticles

Four types of nanoparticles included HA, Ag-HA, Sr-HA, and Ag/Sr-HA were prepared by a hydrothermal method. The Ca/Ag/Sr nitrate solutions were prepared using $Ca(NO_3)_2$•$4H_2O$, $AgNO_3$ and $Sr(NO_3)_2$•$4H_2O$, respectively. $(NH_4)_2HPO_4$ solutions were used as the same phosphorus sources of four synthesized powders. HA was prepared by dissolving $Ca(NO_3)_2$·$4H_2O$ and EDTA disodium in 25 mL deionized water to 11.25 mM and 2.50 mM, respectively, and the pH was adjusted to 10 by NH_3•H_2O (solution 1). Solution 2 was prepared by dissolving $(NH_4)_2HPO_4$ in 25 mL deionized water to 7.50 mM. Solution 1 was stirred for 0.5 h, and then solution 2 was added to solution 1 drop by drop and stirred for 1 h at 60 °C. The pH was regulated and kept at 10 using NH_3•H_2O during the reaction. The mixed solution was transferred to a teflon bottle (100 mL) in a stainless-steel autoclave, and kept under a sealed condition of 180 °C for 12 h. After the reaction was over, the precipitate was centrifuged and washed three times with deionized water and ethanol, respectively. The samples were dried in vacuum at 70 °C overnight. The preparation of Ag-HA, Sr-HA, and Ag/Sr-HA was similar to the synthesis of HA. Different wt.% of Ag and Sr in synthesized samples could be obtained by adjusting the amount of $AgNO_3$ and $Sr(NO_3)_2$•$4H_2O$.

Characterization of the Samples

The crystalline phase of the prepared samples was characterized by X-ray powder diffraction (XRD, D8 Advance, Bruker, Germany). The range of the 2θ angle was from 10 to 60°. The morphology and size of the samples were investigated by a transmission electron microscope (TEM, Tecnai G2 F20, FEI, USA). The length and diameter of the synthesized samples were measured from the TEM images using Nano Measurer software (version 1.2). Fourier transform infrared (FTIR) spectra of samples were measured in KBr pellet on Nicolet iS10 spectrometer (Nicolet iS10, Thermo, USA). The elemental analysis of the prepared powders was analyzed by energy-dispersive X-ray spectroscopy (EDS, PhenomProX, Netherlands Phenom-World, Netherlands).

Table 1 RT-qPCR primer sequence

Target gene	Primer sequence (5′→ 3′)	Anti primer sequence (3′ → 5′)
OCN	AACATGACCAAAAACCAAAAGTG	CATTGTTTCCTGTGTCTTCTGG
Runx2	TTCTCCAACCCACGAATGCAC	CAGGTACGTGTGGTAGTGAGT
ALP	CAGTTTCCAGCGGGTAGGAAG	CCTCATCCCTGACCCTGCAT
BMP2	TGGCCCATTTAGAGGAGAACC	AGGCATGATAGCCCGGAGG
GAPDH	GACTTCAACAGCAACTCCCAC	TCCACCACCCTGTTGCTGTA

Antibacterial Activity Test

The antibacterial activity of Ag-HA and Ag/Sr-HA powders was evaluated by agar disc diffusion method. The Ag-HA or Ag/Sr-HA powders (100 mg) were pressed into thin wafers by tablet press, respectively. The prepared wafers were sterilized by ultraviolet and retained for later use. Escherichia coli (ATCC 25922) and Staphylococcus aureus (ATCC 25923) strains were used for determining the antibacterial effect of synthetic powders. An inoculum of the microorganism was prepared from fresh overnight broth cultures in tripton soy broth with 0.6% yeast extract, which was treated at 37 °C. The agar was poured into petri dishes to form 4-mm thick layers. The layers were dried in the air for 10 min and after that, the diluted bacteria was coated on the plate, and the compressed piece of the samples was attached to it. The agar diffusion test was performed on Muller-Hinton agar. After incubated at 37 °C for 24 h, the antibacterial activity was performed by measuring the inhibition zone around the disc.

Cell Viability Assay

The effects of HA, Ag-HA, Sr-HA, and Ag/Sr-HA on cell viability were tested by MTT assay. MC3T3-E1 cells were cultured in α-MEM with 10% fetal bovine serum in a CO_2 atmosphere at 37 °C and then added in a 96-well plate at a density of 2×10^4 cells/well. After 24-h incubation, the cells were treated with materials in three concentrations (20, 40, and 80 μg/mL) for 1, 4, and 7 days, respectively. After that, the contents in wells were removed and washed with phosphate-buffered saline (PBS), then added of 10 μL of MTT (5 mg/mL) and 90 μL of α-MEM per well. The formazan crystal formation was observed in the well after incubation for 4 h. One hundred microliters of dimethyl sulfoxide (DMSO) was added to each well, and the absorbance was detected by a microplate spectrophotometer at 570 nm (BioRad Model 3550, USA). The cell viability (%) was calculated according to the formula $OD_{sample}/OD_{control} \times 100$.

ALP Activity Assay

For inducing osteogenic differentiation, cells were cultured in α-MEM supplemented with osteogenic differentiation medium (OS, 5 mM β-glycerophosphate, 100 μg/ml ascorbic acid) and 100 nM dexamethasone. Cells were seeded in 48-well plate at a density of 4×10^4 cells per well and exposed to HA, Ag-HA, Sr-HA, and Ag/Sr-HA at a final concentration of 40 μg/mL for 14 days. After the cultural administration, the plates were washed twice with cold PBS, and the cells were lysed by repeated freeze-thaw cycles. An ALP kit was used to measure the expression level of ALP according to the instruction manual, and the total protein content of the cells was measured by a micro-protein assay kit. Each value was normalized to total protein content.

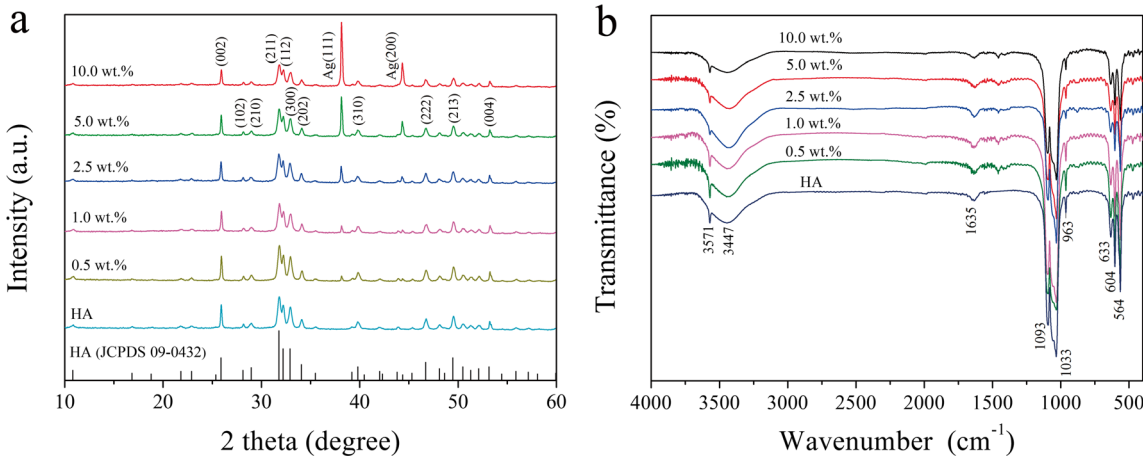

Fig. 1 XRD patterns and FT-IR spectra of HA and different concentrations of Ag-HA powders. **a** XRD patterns. **b** FT-IR spectra

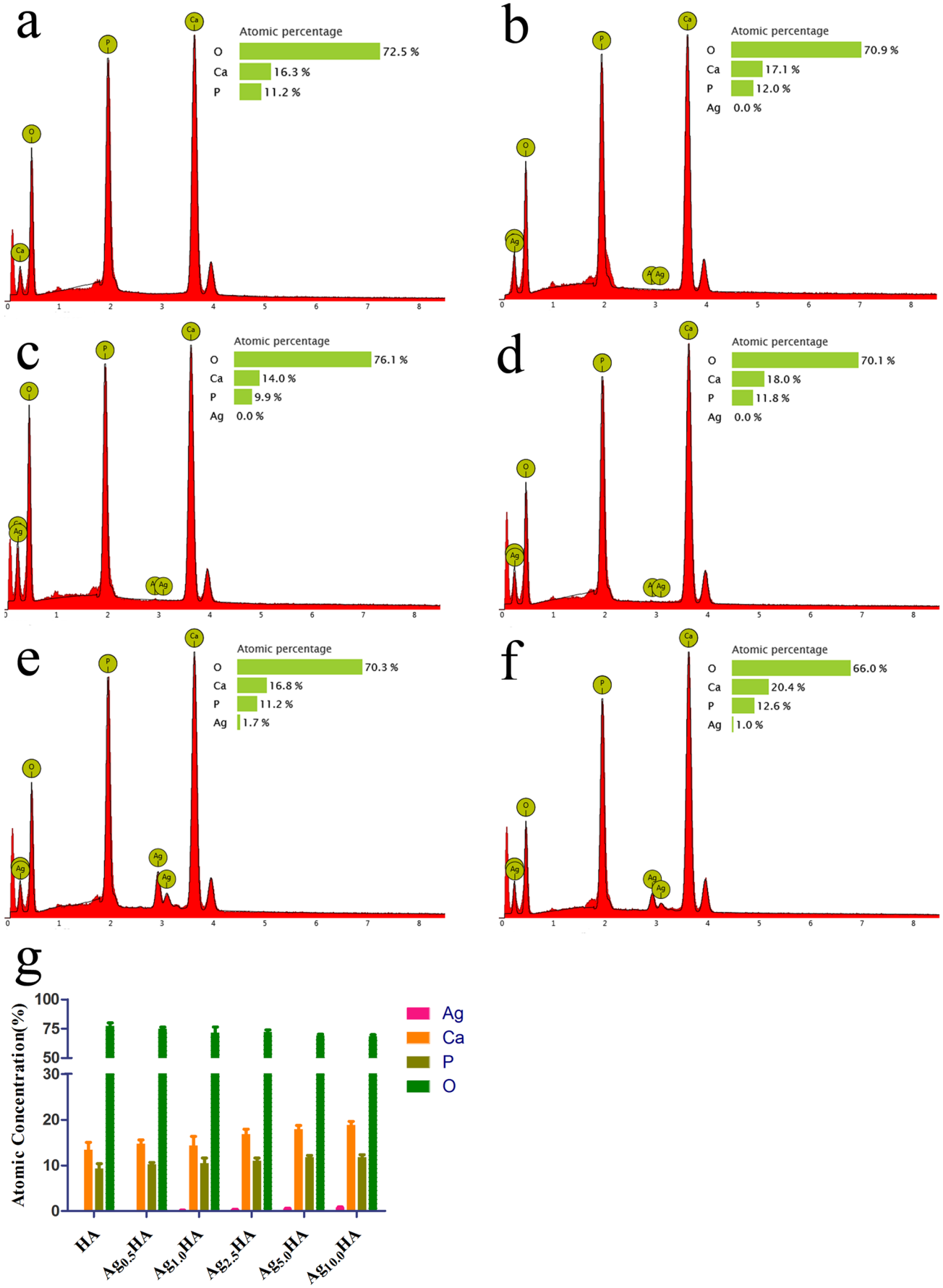
a
Atomic percentage
O 72.5 %
Ca 16.3 %
P 11.2 %
b
Atomic percentage
O 70.9 %
Ca 17.1 %
P 12.0 %
Ag 0.0 %
c
Atomic percentage
O 76.1 %
Ca 14.0 %
P 9.9 %
Ag 0.0 %
d
Atomic percentage
O 70.1 %
Ca 18.0 %
P 11.8 %
Ag 0.0 %
e
Atomic percentage
O 70.3 %
Ca 16.8 %
P 11.2 %
Ag 1.7 %
f
Atomic percentage
O 66.0 %
Ca 20.4 %
P 12.6 %
Ag 1.0 %
g
Atomic Concentration(%)
100
75
50
30
20
10
0
Ag
Ca
P
O
HA
Ag0.5HA
Ag1.0HA
Ag2.5HA
Ag5.0HA
Ag10.0HA

◀ **Fig. 2** The elements of different Ag concentrations of Ag-HA powders. **a** HA. **b** 0.5 wt.% **c** 1.0 wt.%. **d** 2.5 wt.%. **e** 5.0 wt.%. **f** 10.0 wt.%. **g** Quantification of the atomic concentration of elements

Mineralized Matrix Formation Assay

Cells were cultured in 24-well plate at a density of 2×10^6 cells per well with osteogenic differentiation medium OS and HA, Ag-HA, Sr-HA, and Ag/Sr-HA at concentration of 40 μg/mL. The cells were cultured for 21 days, and then washed twice with PBS and fixed with 95% ethanol for 10 min. The ethanol was washed with PBS, and 200 μl ARS (0.1%) was added and incubated for 30 min in an incubator. The orange mineralized nodules were observed and photographed. After taking photographs, 10% (w/v) cetylpyridinium chloride was used to elute the mineralized nodules for 10 min. The absorbance was measured at 570 nm for quantifying the ARS staining at room temperature.

Osteogenic Gene Expression

The expression of four osteogenesis-related genes included osteocalcin (OCN), runt-related transcription factor 2 (Runx2), alkaline phosphatase (ALP), and bone morphogenetic protein-2 (BMP-2) was detected by quantitative reverse transcription polymerase chain reaction (RT-qPCR) (Table 1). GAPDH was used as the housekeeping gene. Briefly, 4×10^4 cells were inoculated per well and cultured with HA, Ag-HA, Sr-HA, and Ag/Sr-HA at final concentration of 40 μg/mL for 14 days. The total cellular RNA was extracted from cells using trizol reagent. All RNA had an A_{260}/A_{280} absorbance ≥ 1.8. cDNA was synthesized from 1 to 3 μg of total RNA using Exscript RTase. Specific primers were used for quantitative RT-qPCR in an ABI Prism 7000 sequence detection system (Applied Biosystems, Foster City, USA). The experiments were performed in triplicate.

Statistical Analysis

Data were presented as mean ± standard deviation (S.D) from three independent experiments. Statistical comparison was analyzed by two-tailed Student's *t* test between different group comparisons. *P* values less than 0.05 were considered to be statistically significant.

Results and Discussion

Characterizations of Pure HA and Ag-HA

The XRD patterns of HA and different concentrations of Ag-HA were shown in Fig. 1a. The main phase in all synthesized samples was identified as hexagonal crystal phase of HA which belonged to space group P63/m (JCPDS No.09-0432). The diffraction peaks corresponding to the (002), (211), (112), (300), (202), (310), (222), (213), and (004) crystal planes were attributed to HA. The diffraction peaks were intense and sharp, and there were no other undesirable peaks in the synthesized powders. In addition to the peaks originated from HA, the peaks at 38.1°and 44.3° can be attributed to elemental Ag (JCPDS No. 87-0179) in the XRD patterns of Ag-HA. FTIR spectroscopic analysis was carried out to identify the functional groups of synthesized powders. The FT-IR spectra of HA and different concentrations of Ag-HA were shown in Fig. 1b. The absorption bands at 469 cm^{-1} (ν_2), 564 and 604 cm^{-1} (ν_4), 963 cm^{-1} (ν_1), and 1033 cm^{-1} and 1093 cm^{-1} (ν_3) were attributed to the phosphate groups (PO_4^{3-}). The peaks at 1635 cm^{-1} correspond to hydrogen phosphate (HPO_4^{2-}). The peaks appeared at 3447 and 3571 cm^{-1} were

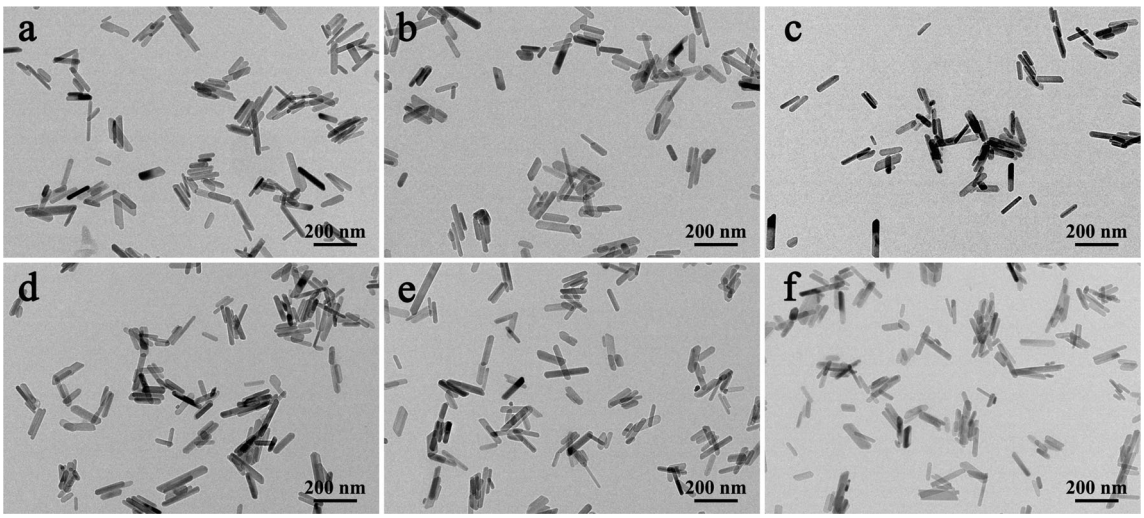

Fig. 3 TEM images of HA and different Ag concentrations of Ag-HA powders. **a** HA. **b** 0.5 wt.%. **c** 1.0 wt.%. **d** 2.5 wt.%. **e** 5.0 wt.%. **f** 10.0 wt.%

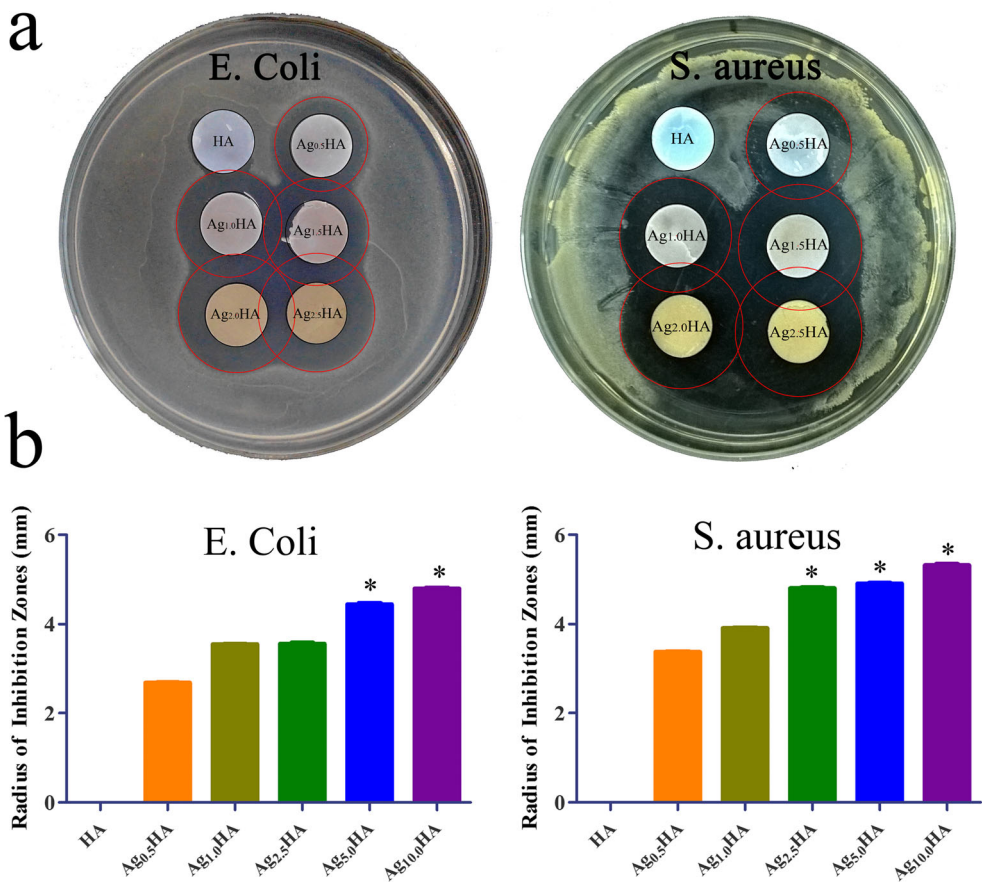

Fig. 4 Inhibition zone of HA and different Ag concentrations of Ag-HA powders to E. coli and S. aureus by the disc diffusion assay. **a** Inhibition zone of different samples. **b** Quantification of the inhibition zones of different samples. $^{*}P < 0.05$ compared with the corresponding $Ag_{0.5}HA$ group

ascribed to the characteristic tensile vibrational mode of the adsorbed water and structural -OH groups on the surface of the synthesized powders [23]. The FTIR spectra of different Ag concentrations of Ag-HA were similar to those of HA. There is no significant difference in the shapes and intensities of the peaks. It suggested that the substitution of Ag had no change on the structure of the pure HA. This was consistent with the previous report [15]. The chemical elements of calcium (Ca), phosphorous (P), oxygen (O), and silver (Ag) were found in Ag-HA by EDS analysis (Fig. 2). The morphology and size of the HA and different concentrations of Ag-HA were investigated by TEM. TEM micrographs gave the direct information about the size and shape of the synthesized samples. Both pure HA and Ag-HA exhibited a rod-like morphology with a relatively narrow size distribution. The length of Ag-HA was about 180.5 ± 17.9 nm and the diameter was about 21.2 ± 3.1 nm (Fig. 3). The results showed that substitution of Ag in HA had no effect on the morphology of HA.

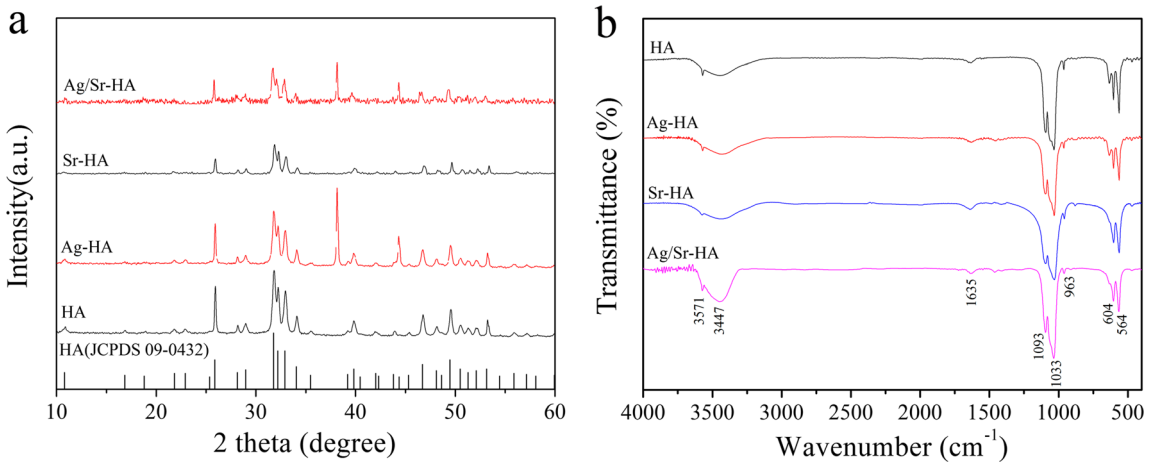

Fig. 5 XRD patterns and FT-IR spectra of the synthesized HA, Ag-HA, Sr-HA, and Ag/Sr-HA nanopowders. **a** XRD patterns. **b** FT-IR spectra

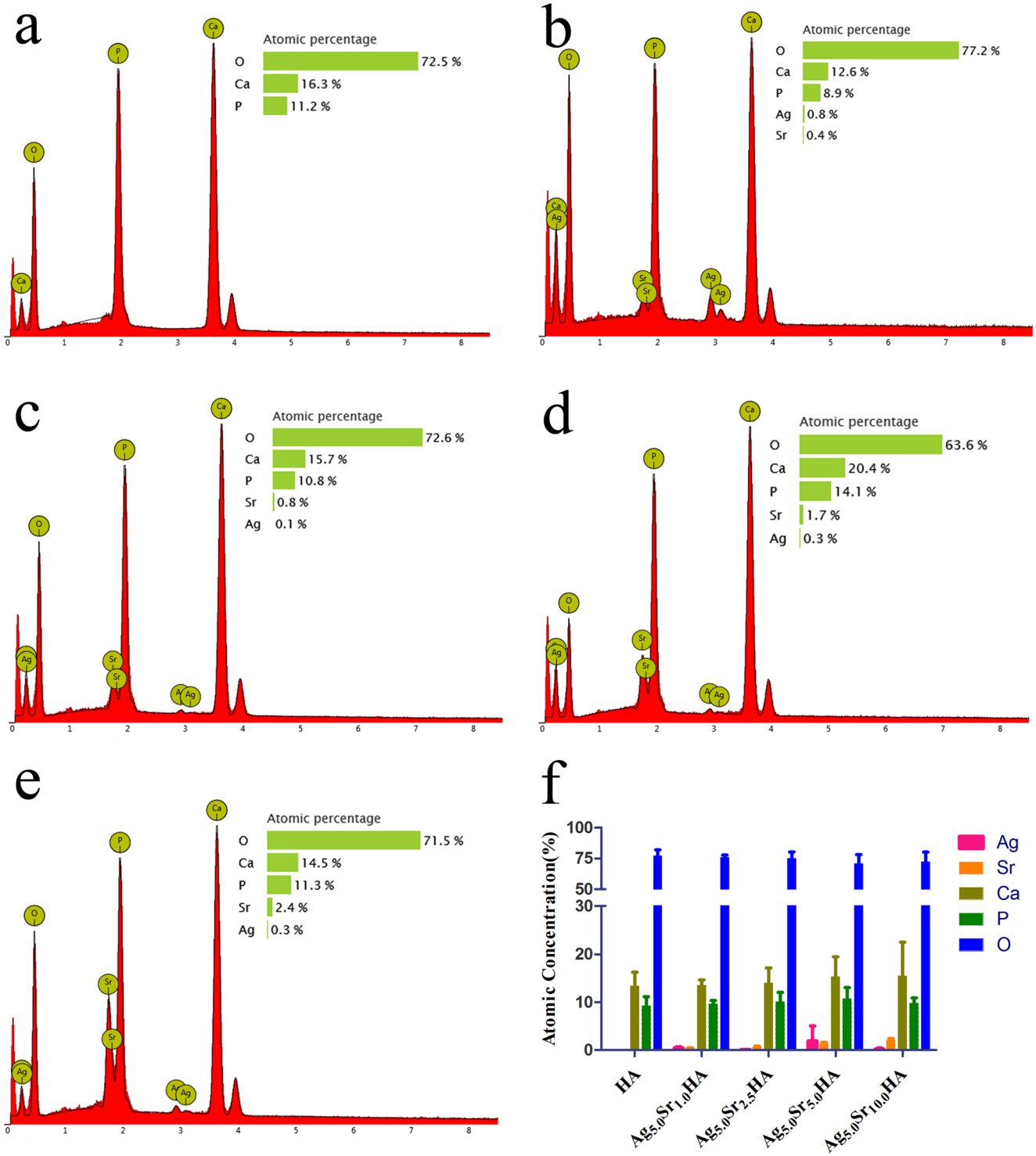

Fig. 6 The elements of different Sr concentrations of Ag/Sr-HA powders. **a** 1.0 wt.%. **b** 2.5 wt.%. **c** 5.0 wt.%. **d** 10.0 wt.%. **f** Quantification of the atomic concentration of elements

Antibacterial Property of Ag-HA

The agar disc diffusion method was used to detect antimicrobial activities of HA and Ag-HA. The inhibition zone of HA and different concentrations of Ag-HA against E. coli and S. aureus was shown in Fig. 4a. It was found that higher concentration (5.0 and 10.0 wt.%) of Ag-HA exhibited effective antibacterial activity with a 4-6-mm inhibition zone. However, pure HA had no bactericidal property against bacterial strains. The Ag-HA had stronger antimicrobial activity than pure HA, and the antimicrobial activity of Ag-HA was enhanced with

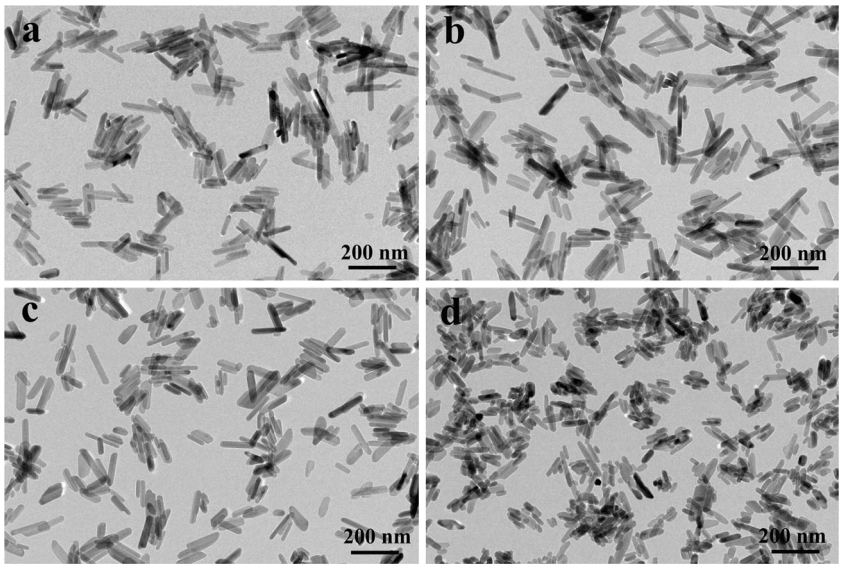

Fig. 7 TEM images of different Sr concentrations of Ag/Sr-HA powders. **a** 1.0 wt.%. **b** 2.5 wt.%. **c** 5.0 wt.%. **d** 10.0 wt.%

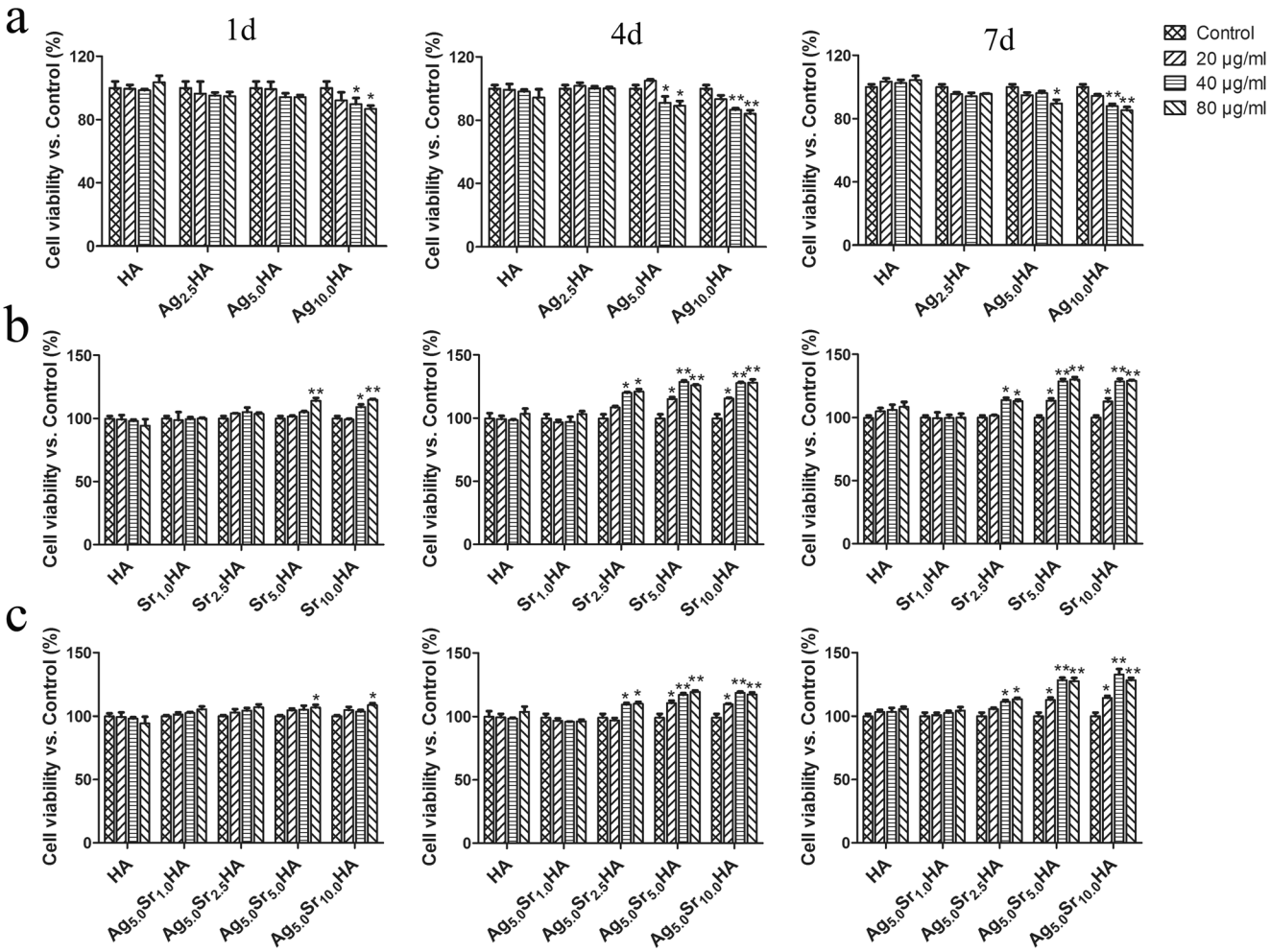

Fig. 8 Effects of the synthesized HA, Ag-HA, Sr-HA, and Ag/Sr-HA nanopowders on the MC3T3-E1 cell viability. **a** Ag-HA. **b** Sr-HA. **c** Ag/Sr-HA. Data are expressed as means ± standard deviation from three independent experiments ($n = 6$). $^{**}P < 0.01$, $^{*}P < 0.05$ compared with the control group

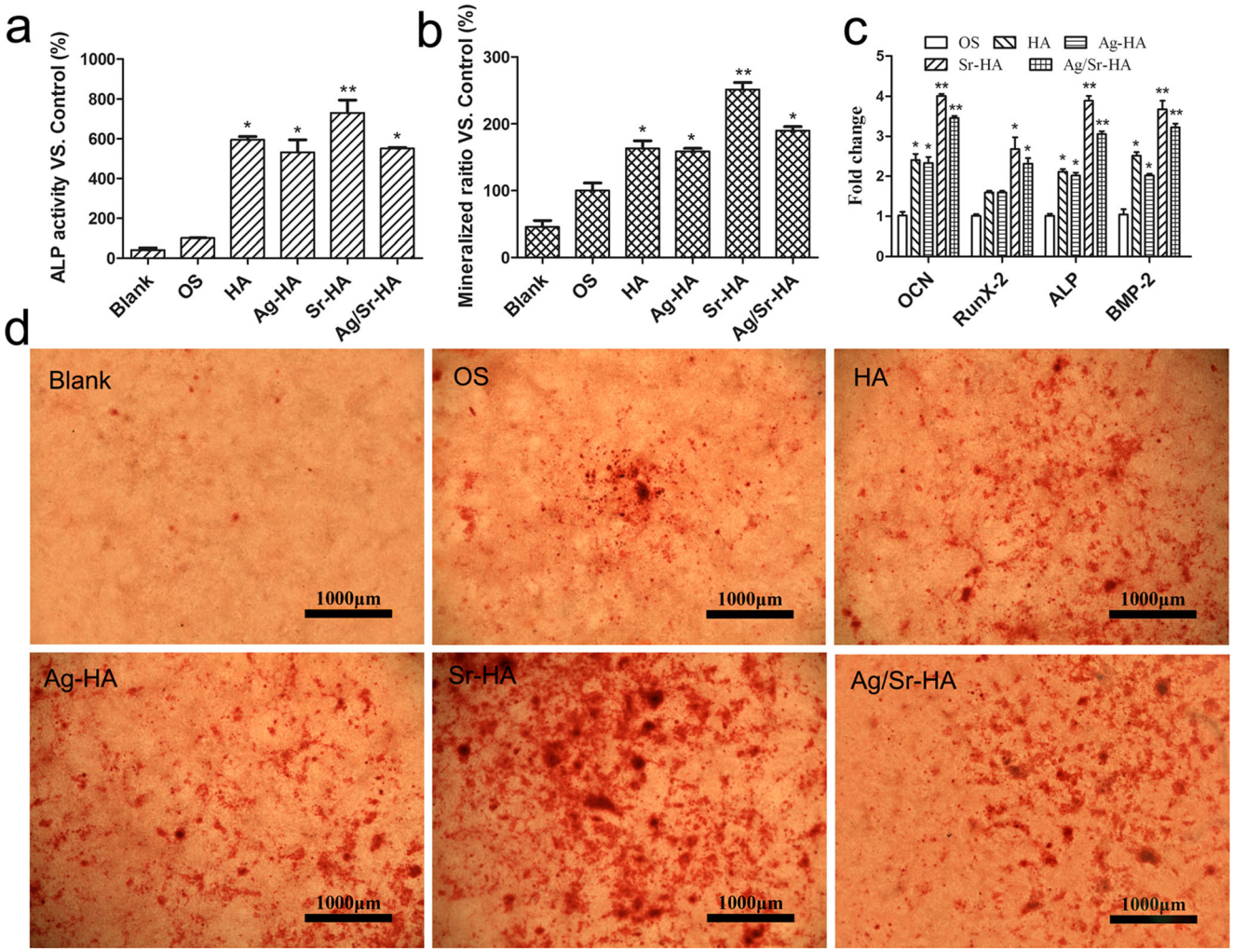

Fig. 9 Effects of the synthesized HA, Ag-HA, Sr-HA, and Ag/Sr-HA nanopowders on the cells differentiation of MC3T3-E1 cells. **a** ALP activity of cells. **b** Quantification of the mineralized matrix of cells. **c** The expression of mRNA for OCN, Runx-2, ALP, and BMP-2 in cells. **d** The mineralized matrix nodules of cells stained by ARS. Data are expressed as means ± standard deviation from three independent experiments ($n = 6$). $^{**}P < 0.01$, $^{*}P < 0.05$ compared with the corresponding OS group.

the increasing Ag concentration in HA. It seemed that the antibacterial effect of Ag-HA (5.0 wt.%) was better than that of Ag-HA (0.5 and 1.0 wt.%). So the Ag/Sr-HA used in following experiments had a fixed concentration of Ag (5.0 wt.%) and different concentrations of Sr. Therefore, it was concluded that Ag played a key role in the excellent antibacterial action of Ag-HA.

Characterizations of Ag/Sr-HA

The XRD patterns of Ag/Sr-HA were shown in Fig. 5a. It was found that the Ag/Sr-HA exhibited similar peaks to that of Ag-HA. However, the 2θ values of Ag/Sr-HA sample were slightly different from that of Ag-HA. The peak shift may due to the different ionic radius of Sr (1.13 Å) and Ca (0.99 Å). The lattice parameters would be changed with the incorporation of ions, such as Mg^{2+}, Zn^{2+}, and Ba^{2+}, which were different from the ionic radius of Ca^{2+} [24–26]. The EDS spectra also indicated that the Sr had been incorporated into Ag-HA structure (Fig. 6). The FT-IR spectra of HA, Ag-HA, Sr-HA, and Ag/Sr-HA were shown in Fig. 5b. The FTIR spectra of Ag/Sr-HA were similar to that of Ag-HA. After co-substitution of Sr into Ag-HA, the shape and intensity of the peaks have no change significantly. The TEM images of different Sr concentrations of Ag/Sr-HA were shown in Fig. 7. After co-substitution of lower Sr concentrations (1.5, 2.5, and 5.0 wt.%), Ag/Sr-HA had regular nanoparticle morphology with good crystallinity. The morphology of Ag/Sr-HA had no remarkable change. The length of Ag/Sr-HA was about 175.8 ± 18.5 nm and the diameter was about 18.3 ± 2.6 nm. But the morphology became slightly irregular when the Sr concentration up to 10.0 wt.% (Fig. 7d). It indicated that the lower crystallinity due to the incorporation of higher concentration of Sr in Ag-HA. After the Ca in crystal lattice of HA was replaced by Sr, the lattice constant, cell volume, and density of HA were increased linearly. The crystallinity and

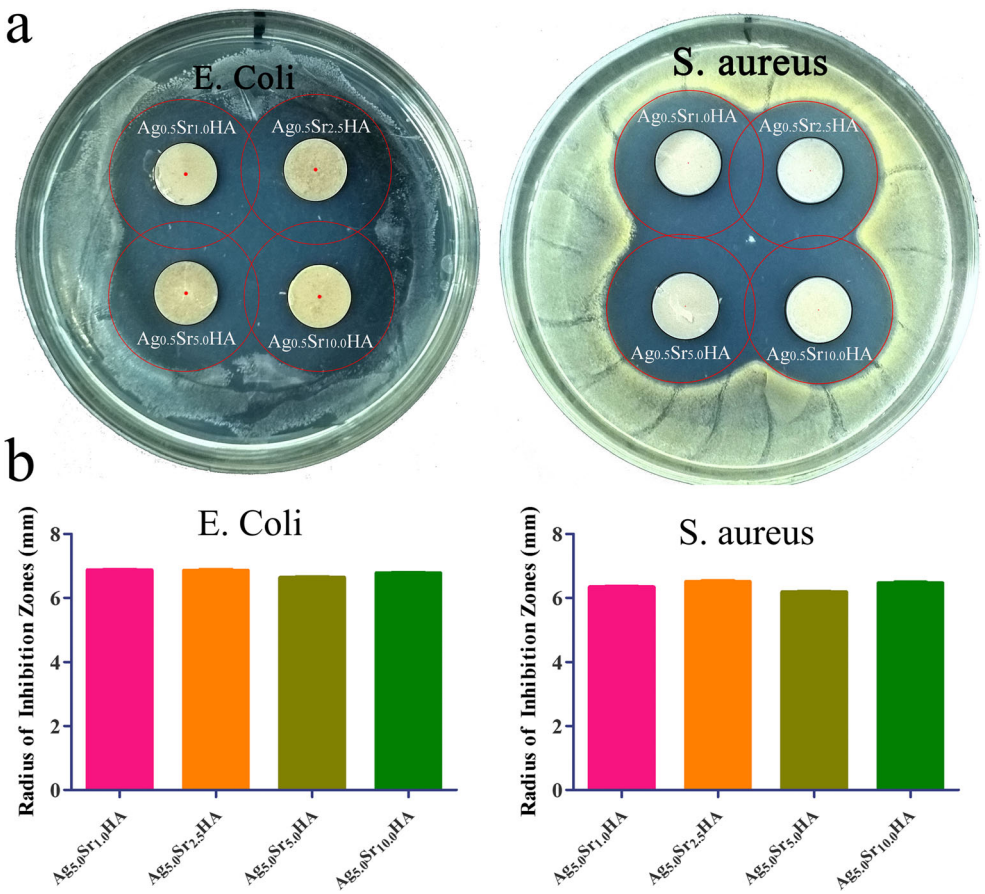

Fig. 10 Inhibition zone of different Sr concentrations of Ag/Sr-HA powders to E. coli and S. aureus by the disc diffusion assay. **a** Inhibition zone of different samples. **b** Quantification of the inhibition zones of different samples

morphology of HA may change to a certain extent. The reason might be that Sr has a larger ionic radius than Ca [27]. So the concentration of Sr of Ag/Sr-HA used in following ALP activity and mineralized matrix formation experiments was fixed to 5.0 wt.%.

Effects of Synthesized Samples on Cell Viability

The results of the cell viability assay showed that the HA and Ag-HA nanoparticles almost had no toxicity on cells. The cell viability was similar to that of control group after treated by HA and Ag-HA (2.5 and 5.0 wt.%) nanoparticles (Fig. 8a). It indicated that lower Ag doped in HA had no toxicity. As the concentration of Ag increased to 10.0 wt.%, the samples exhibited a certain degree of cytotoxicity which was proved by the lowered cell viability compared to the HA group. This result was consistent with earlier studies that the higher Ag concentration of Ag-HA exhibited cytotoxicity, resulting in cell proliferation limitation and cell death [28]. Therefore, it can be concluded that the Ag-HA nanoparticles containing a small quantity of Ag were more appropriate for applications in implant. Compared with pure HA, the Sr-HA and Ag/Sr-HA nanoparticles can promote cell proliferation more effectively. All samples can improve cell viability after training 4 days to 7 days (Fig. 8b, c). The incorporation of Sr in HA plays a key role in the cell proliferation. It has demonstrated that Sr^{2+} ions may stimulate phosphorylation of extracellular signal-regulated kinase (ERK) in mouse osteoblastic MC3T3-E1 cells expressing the calcium sensing receptor (CaR) endogenously, and thus enhance the mRNA expression of osteocalcin and bone morphogenetic protein-2 in MC3T3-E1 cells, promote cell proliferation and mineralization [29].

Effects of Synthesized Samples on Osteogenic Differentiation

The effects of synthesized nanopowders on osteogenic differentiation of MC3T3-E1 cells in vitro were investigated through ALP activity assay, Alizarin Red staining (ARS) and RT-qPCR analysis. As an early stage marker of osteogenic differentiation of MC3T3-E1 [30], ALP activity was evaluated quantitatively. The ALP activity of MC3T3-E1 cells cultured with different nanopowders for 14 days was shown in Fig. 9a. The ALP level of several nanopowders group was strongly increased than that of OS group. The Sr ions in hydroxyapatite had a significant stimulatory effect on ALP activity. The mineralization product serves as a late stage marker of osteogenic differentiation. The cellular mineralization was tested at prolonged culture periods of up to 21 days by Alizarin

red staining (ARS) and quantitative mineralization assay. The mineralized matrix nodules of cells and quantification of the stained extracts were shown in Fig. 9b, d. The mineralization promotion rate was in the sequence: Sr-HA > Ag/Sr-HA > HA > Ag-HA > OS > Blank. It was indicated that Sr element could further enhance nodule formation and calcium deposition while reducing silver cytotoxicity.

The gene expression of osteogenic markers was evaluated by RT-qPCR method. The expression of OCN, Runx-2, ALP, and BMP-2 plays a key role in the progress of osteogenic differentiation. In order to further investigate the effects of synthesized nanopowders on osteogenic differentiation of MC3T3-E1 cells at the molecular biological level, the gene expression of cells was detected after cultured with different nanopowders for 14 days. The expression levels of OCN, Runx-2, ALP, and BMP-2 were increased in four synthesized nanopowder groups than that of OS group (Fig. 9c). Furthermore, the Sr-HA and Ag/Sr-HA particularly promoted genes expression involved in bone formation. The results indicated that Sr element can enhance a series of cellular response included proliferation, differentiation, and mineralization of osteoblasts in vitro, which agreed with previous studies [31–33].

Antibacterial Property of Ag/Sr-HA

The antibacterial activity of different Sr concentrations of Ag/Sr-HA was shown in Fig. 10. The results indicated that the synthesized Ag/Sr-HA had excellent antibacterial activity against E. coli and S. aureus. The antibacterial activity of Ag/Sr-HA was a little higher than that of Ag-HA. The inhibition zone of Ag/Sr-HA was about 6–7 mm, whereas the inhibition zone of 5.0 wt.% Ag-HA was found to be around 4–5 mm. It was possible that co-substitution of Sr improved the antibacterial property of Ag-HA. The antibacterial ability of Ag/Sr-HA had no dose-dependent relationship with increasing concentration of Sr.

Conclusion

In summary, a novel Ag/Sr-HA nanopowder with osteogenic and antibacterial activity was synthesized by hydrothermal method. The power exhibited excellent osteoinductive activity, and displayed better antibacterial activity against E. coli and S. aureus in vitro. The formation of Ag-HA and Ag/Sr-HA nanopowder was revealed clearly by structural characterization. The incorporation of Ag in HA improved antibacterial activity of HA significantly. As a second element, Sr alleviated the cytotoxicity of Ag to osteoblasts. Hence, the co-substitution of Sr in Ag-HA counteracted the toxicity of Ag though enhancing cell viability. So the biocompatibility of Ag/Sr-HA was improved by optimizing the ratio of two elements included Ag and Sr. Therefore, these synthesized materials can help to develop more effective bone implants, due to their excellent osteogenic properties as well as antibacterial characteristics.

Funding This work was supported by the National Natural Science Foundation of China (21471044), the Natural Science Foundation of Hebei Province (B2020201020), the Science and Technology Projects of Hebei Education Department (ZD2020150), the Third Batch of Top Youth Talent Support Program of Hebei Province, the Priority Strategy Project of Key Laboratory of Medicinal Chemistry and Molecular Diagnosis of Ministry of Education (ts2019006), Medical Science Foundation of Hebei University (2020A03), and the Post-graduate's Innovation Fund Project of Hebei University (hbu2020ss012).

Declarations

Conflict of Interest The authors declare no competing interests.

References

1. Habraken W, Habibovic P, Epple M, Bohner M (2016) Calcium phosphates in biomedical applications: materials for the future. Mater Today 19:69–87. https://doi.org/10.1016/j.mattod.2015.10.008
2. Guha AK, Singh S, Kumaresan R, Nayar S, Sinha A (2009) Mesenchymal cell response to nanosized biphasic calcium phosphate composites. Colloids Surf B Biointerfaces 73:146–151. https://doi.org/10.1016/j.colsurfb.2009.05.009
3. Ruchholtz S, Täger G, Nastkolb D (2004) The infected hip prosthesis. Unfallchirurg 107:307–317. https://doi.org/10.1007/s00113-004-0751-9
4. Huang Y, Ding Q, Han S, Yan Y, Pang X (2013) Characterisation, corrosion resistance and in vitro bioactivity of manganese-doped hydroxyapatite films electrodeposited on titanium. J Mater Sci Mater Med 24:1853–1864. https://doi.org/10.1007/s10856-013-4955-9
5. Campoccia D, Montanaro L, Arciola CR (2006) The significance of infection related to orthopedic devices and issues of antibiotic resistance. Biomaterials 27:2331–2339. https://doi.org/10.1016/j.biomaterials.2005.11.044
6. Anghelina FV, Ungureanu DN, Bratu V, Popescu IN, Rusanescu CO (2013) Fine structure analysis of biocompatible ceramic materials based hydroxyapatite and metallic biomaterials 316 L. Appl Surf Sci 285:65–71. https://doi.org/10.1016/j.apsusc.2013.06.102
7. Riaz M, Zia R, Saleemi F, Ikram H, Bashir F (2015) In vitro antimicrobial activity of ZnO based glass-ceramics against pathogenic bacteria. J Mater Sci Mater Med 26:268–279. https://doi.org/10.1007/s10856-015-5603-3
8. Qin Q, Li J, Wang J (2016) Antibacterial activity comparison of three metal oxide nanoparticles and their dissolved metal ions. Water Environ Res 89:378–383. https://doi.org/10.2175/106143017X14839994523262
9. Gabriel JS, Gonzaga VAM, Poli AL, Schmitt CC (2017) Photochemical synthesis of silver nanoparticles on chitosans/montmorillonite nanocomposite films and antibacterial activity. Carbohyd Polym 171:202–210. https://doi.org/10.1016/j.carbpol.2017.05.021
10. Karbowniczek J, Cordero-Arias L, Virtanen S, Misra SK, Valsami-Jones E, Tuchscherr L, Rutkowski B, Górecki K, Bała P, Czyrska-

Filemonowicz A (2017) Electrophoretic deposition of organic/inorganic composite coatings containing ZnO nanoparticles exhibiting antibacterial properties. Mater Sci Eng C 77:780–789. https://doi.org/10.1016/j.msec.2017.03.180

11. Azeena S, Subhapradha N, Selvamurugan N, Narayan S, Srinivasan N, Murugesan R, Chung TW, Moorthi A (2016) Antibacterial activity of agricultural waste derived wollastonite doped with copper for bone tissue engineering. Mater Sci Eng C 71:1156–1165. https://doi.org/10.1016/j.msec.2016.11.1180
12. Kunkalekar RK, Prabhu MS, Naik MM, Salker AV (2014) Silver-doped manganese dioxide and trioxide nanoparticles inhibit both gram positive and gram negative pathogenic bacteria. Colloids Surf B Biointerfaces 113:429–434. https://doi.org/10.1016/j.colsurfb.2013.09.036
13. Peetsch A, Greulich C, Braun D, Stroetges C, Rehage H, Siebers B, Koller M, Epple M (2013) Silver-doped calcium phosphate nanoparticles: synthesis, characterization, and toxic effects toward mammalian and prokaryotic cells. Colloids Surf B Biointerfaces 102:724–729. https://doi.org/10.1016/j.colsurfb.2012.09.040
14. Jamuna-Thevi K, Bakar SA, Ibrahim S, Shahab N, Toff MRM (2011) Quantification of silver ion release, in vitro cytotoxicity and antibacterial properties of nanostuctured Ag doped TiO_2 coatings on stainless steel deposited by RF magnetron sputtering. Vacuum 86:235–241. https://doi.org/10.1016/j.vacuum.2011.06.011
15. Gopi D, Shinyjoy E, Kavitha L (2014) Synthesis and spectral characterization of silver/magnesium co-substituted hydroxyapatite for biomedical applications. Spectrochim Acta A 127:286–291. https://doi.org/10.1016/j.saa.2014.02.057
16. Jin GD, Qin H, Cao HL, Qian S, Zhao YC, Peng XC, Zhang XL, Liu XY, Chu PK (2014) Synergistic effects of dual Zn/Ag ion implantation in osteogenic activity and antibacterial ability of titanium. Biomaterials 35:7699–7713. https://doi.org/10.1016/j.biomaterials.2014.05.074
17. Bari A, Bloise N, Fiorilli S, Novajra G, Vallet-Regí M, Bruni G, Torres-Pardo A, González-Calbet JM, Visai L, Vitale-Brovarone C (2017) Copper-containing mesoporous bioactive glass nanoparticles as multifunctional agent for bone regeneration. Acta Biomater 55:493–504. https://doi.org/10.1016/j.actbio.2017.04.012
18. Liu J, Rawlinson SC, Hill RG, Fortune F (2016) Strontium-substituted bioactive glasses in vitro osteogenic and antibacterial effects. Dent Mater 32:412–422. https://doi.org/10.1016/j.dental.2015.12.013
19. Gentleman E, Fredholm YC, Jell G, Lotfibakhshaiesh N, O'Donnell MD, Hill RG, Stevens MM (2010) The effects of strontium-substituted bioactive glasses on osteoblasts and osteoclasts in vitro. Biomaterials 31:3949–3956. https://doi.org/10.1016/j.biomaterials.2010.01.121
20. Yang F, Tu J, Yang D, Li G, Cai L, Wang L (2010) Osteogenic differentiation of mesenchymal stem cells could be enhanced by strontium. Eng Med Biol Soc 2010:823–826. https://doi.org/10.1109/IEMBS.2010.5626774
21. Atkins GJ, Welldon KJ, Halbout P, Findlay DM (2009) Strontium ranelate treatment of human primary osteoblasts promotes an osteocyte-like phenotype while eliciting an osteoprotegerin response. Osteopor Int 20:653–664. https://doi.org/10.1007/s00198-008-0728-6
22. Lei Y, Xu Z, Ke Q, Yin W, Chen Y, Zhang C, Guo Y (2017) Strontium hydroxyapatite/chitosan nanohybrid scaffolds with enhanced osteoinductivity for bone tissue engineering. Mater Sci Eng C 72:134–142. https://doi.org/10.1016/j.msec.2016.11.063
23. Kheradmandfard M, Fathi MH (2013) Fabrication and characterization of nanocrystalline Mg-substituted fluorapatite by high energy ball milling. Ceram Int 39:1651–1658. https://doi.org/10.1016/j.ceramint.2012.08.007
24. Bigi A, Falini G, Foresti E, Gazzano M, Ripmonti A, Roveri N (1996) Rietveld structure refinements of calcium hydroxylapatite containing magnesium. Acta Crystallogr B 52:87–92. https://doi.org/10.1107/S0108768195008615
25. Ren F, Xin R, Ge X, Leng Y (2009) Characterization and structural analysis of zinc-substituted hydroxyapatites. Acta Biomater 5:3141–3149. https://doi.org/10.1016/j.actbio.2009.04.014
26. Xiu ZL, Lü MK, Liu SW, Zhou GJ, Su BY, Zhang HP (2005) Barium hydroxyapatite nanoparticles synthesized by citric acid sol–gel combustion method. Mater Res Bull 40:1617–1622. https://doi.org/10.1016/j.materresbull.2005.04.033
27. Wang LP, Pathak JL, Liang DL, Zhong NY, Guan HB, Wan MJ, Miao GH, Li ZM, Ge LH (2020) Fabrication and characterization of strontium- hydroxyapatite/silk fibroin biocomposite nanospheres for bone-tissue engineering applications. Int J Biol Sci 142:366–375. https://doi.org/10.1016/j.ijbiomac.2019.09.107
28. Roy M, Fielding GA, Beyenal H, Bandyopadhyay A, Bose S (2012) Mechanical, in vitro antimicrobial and biological properties of plasma sprayed silver-doped hydroxyapatite coating. ACS Appl Mater Interfaces 4:1341–1349. https://doi.org/10.1021/am201610q
29. Takaoka S, Yamaguchi T, Yano S, Yamauchi M, Sugimoto T (2010) The Calcium-sensing Receptor (CaR) is involved in strontium ranelate-induced osteoblast differentiation and mineralization. Horm Metab Res 42:627–631. https://doi.org/10.1055/s-0030-1255091
30. Gaharwar AK, Mihaila SM, Swami A, Patel A, Sant S, Reis RL, Marques AP, Gomes ME, Khademhosseini A (2013) Bioactive silicate nanoplatelets for osteogenic differentiation of human mesenchymal stem cells. Adv Mater 25:3329–3336. https://doi.org/10.1002/adma.201300584
31. Zhao LZ, Wang HR, Huo KF, Zhang XM, Wang W, Zhang YMWZF, Chu PK (2013) The osteogenic activity of strontium loaded titania nanotube arrays on titanium substrates. Biomaterials 34:19–29. https://doi.org/10.1016/j.biomaterials.2012.09.041
32. Xu K, Chen W, Mu C, Yu Y, Cai K (2017) Strontium folic acid derivative functionalized titanium surfaces for enhanced osteogenic differentiation of mesenchymal stem cells in vitro and bone formation in vivo. J Mater Chem B 5:6811–6826. https://doi.org/10.1039/C7TB01529A
33. Xing M, Wang X, Wang E, Gao L, Chang J (2018) Bone tissue engineering strategy based on the synergistic effects of silicon and strontium ions. Acta Biomater 72:381–395. https://doi.org/10.1016/j.actbio.2018.03.051